ELSEVIER

Polymer 43 (2002) 803–812

polymer

www.elsevier.com/locate/polymer

Spatial gradients in particle reinforced polymers characterized by X-ray attenuation and laser confocal microscopy

R.R. Lagasse[a,*], K.R. Thompson[b]

[a]Organic Materials Department, Sandia National Laboratories, Albuquerque, NM 87185-1411, USA
[b]Experimental Structural Mechanics Department, Sandia National Laboratories, Albuquerque, NM 87185-0555, USA

Received 9 April 2001; received in revised form 10 September 2001; accepted 12 September 2001

Abstract

The goal of this work is to develop techniques for measuring gradients in particle concentration within filled polymers, such as thermosetting polymer encapsulants. A high concentration of filler particles is added to such materials to tailor physical properties such as thermal expansion coefficient. Sedimentation and flow-induced migration of particles can produce concentration gradients that are most severe near boundaries. Therefore, techniques for measuring local particle concentration should be accurate near boundaries. Particle gradients in an alumina-filled epoxy resin are measured with a spatial resolution of 0.2 mm using an X-ray beam attenuation technique, but an artifact reduces accuracy near the specimen's edge. Local particle concentration near an edge can be measured more reliably using microscopy coupled with image analysis. This is illustrated by measuring concentration profiles of glass particles having 40 μm median diameter using images acquired with a confocal laser fluorescence microscope. The mean of the measured profiles of volume fraction agrees to better than 3% with the expected value and the shape of the profiles agrees qualitatively with simple theory for sedimentation of monodisperse particles. Evidence that the microscopic method can be extended to smaller particles is provided by local concentration measurements on an epoxy polymer containing particles having diameters of the order of 1 μm.

Keywords: Composite; Filler; Particle

1. Introduction

Many polymeric materials used in engineering applications contain a high concentration of particulate modifiers. For example, polymer encapsulants for electronic devices are modified with ~50 vol.% of oxide particles, often silica, in order to reduce the thermal expansion coefficient [1]. One application having current interest is the Direct-Chip-Attachment packaging scheme in which an encapsulant fills the gap between the chip and substrate. Spatially uniform distribution of particles is desired to achieve spatially uniform encapsulant properties, such as thermal expansion coefficient and elastic modulus. A uniform distribution of particles is also desired in order to simplify modeling flow of these materials [2]. The present investigation is aimed at developing techniques for determining the spatial uniformity of particle concentration in highly filled polymers.

One of the mechanisms producing a spatial gradient in concentration is sedimentation (or flotation) of particles differing in density from the polymer when it is in a fluid state. This can cause large changes in particle concentration over small distances, often near fluid boundaries. To clarify that statement, consider the simplest case of uniformly sized particles large enough that hydrodynamic and gravitational forces dominate over interparticle forces, in a fluid having spatially uniform particle concentration, φ_0, as an initial condition. We consider the instructive, but unrealistic case (see Section 5) where the sedimentation velocity of all particles is the same and independent of local concentration. For this case, sedimentation will produce three zones of particle concentration [3,4], as shown in Fig. 1(a). Here, a sediment having volume fraction φ_{max} forms at the lower fluid boundary. φ_{max} is the concentration where viscosity is so high that the suspension behaves like a solid (occurring at volume fraction 0.63 for random close packed monodisperse spheres [5]). Fig. 1(a) shows that sedimentation produces *discontinuous steps in particle concentration* at the two boundaries separating three different zones: the sediment, a middle zone having uniform concentration equal to the initial value and a particle-free, clear zone. A simple mass balance relates the thickness of the sediment and the clear zone

$$t_{sed} = t_{clear} \frac{\varphi_0}{\varphi_{max} - \varphi_0} \quad (1)$$

* Corresponding author. Fax: +1-505-844-9781.
E-mail address: rrlagas@sandia.gov (R.R. Lagasse).

0032-3861/02/$ - see front matter
PII: S0032-3861(01)00637-1

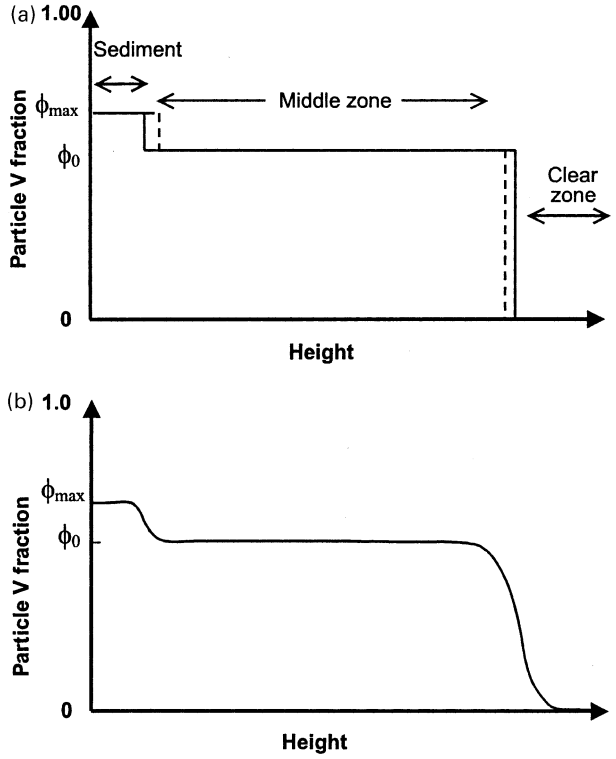

Fig. 1. Schematic representation of particle concentration profiles produced by sedimentation. (a) Profiles produced by uniform size particles having sedimentation velocity independent of local concentration at shorter and longer sedimentation times (solid and dashed lines, respectively). (b) Sigmoidal profiles produced by more realistic, polydisperse particles whose sedimentation velocity depends on local concentration.

As sedimentation proceeds, the thicknesses of the sediment and clear zone increase, as indicated by the dashed lines.

In a more realistic case, where the sedimentation velocity depends on local particle concentration [3,4], and where the particles have a range of sizes (therefore, a range of velocities), the gradient in concentration at the boundaries will be very high instead of infinite, as shown in Fig. 1(b). At early stages of sedimentation, the two transition regions having very high concentration gradient will be close to the top and bottom boundaries of the fluid. This case of minimal sedimentation is relevant since it is expected that technologically important materials will be formulated to minimize the extent of sedimentation (in order to produce spatially uniform properties). Therefore, a technique measuring particle concentration profiles in such a material must be reliable near its boundaries.

Two additional mechanisms producing gradients in particle concentration, are related to flow. Since these phenomena are driven by hydrodynamic, and not gravitational forces, they are operative even when the particles are neutrally buoyant. One mechanism is particle migration normal to the flow direction in a sheared suspension, from regions of high to low shear rate [6]. For the case of shearing flow through a channel, the region of highest shear rate, and therefore the region of particle depletion, is near the channel wall. The second mechanism is accumulation of particles near an advancing free surface when a suspension flows into a cavity [7]. Similar to sedimentation, both the mechanisms can produce large gradients in particle concentration near boundaries.

The objective of the present work is to develop techniques for measuring spatial profiles in particle concentration in highly filled polymers over distances of the order 100 μm, especially near boundaries. Most of the experiments utilize particles having diameters ranging from 1 to 100 μm. Extension to smaller particles is considered near the end. In one case, the polymer constituent contains particles of a second, immiscible polymeric additive that need to be distinguished from filler particles. The measurement techniques are validated using specimens that have experienced sedimentation (without significant flow), since sedimentation-derived concentration profiles can be predicted [3,4], at least qualitatively.

2. Experimental

2.1. Materials

Important characteristics of the reinforcing particles are listed in Table 1. The distribution of diameters for each of the powders was measured via Mie analysis of angularly dependent scattered light (using an LS230 instrument from Coulter Corp.) In the table, D_{50} is the median of the volume distribution of particle sizes, i.e. the diameter at which half of the total volume of particles is smaller and half larger. The D_{10} and D_{90} values have corresponding definitions. D_{SV} is a different kind of average diameter, defined below. The alumina was a ground tabular product having irregular particle shape and a broad size distribution,

Table 1
Reinforcing particles

Identifier	Nominal composition	Particle density (g/cc)	Size distribution range (μm)			D_{SV} (μm)
			D_{10}	D_{50}	D_{90}	
Alumina	Al_2O_3	3.92	2	12	34	
Solid glass	A-glass	2.45	28	40	56	38
Hollow glass	Borosilicate glass	0.32	24	41	62	37
Silica	SiO_2	2.21	0.6	2.2	4.7	

indicated by the large spread between the D_{10} and D_{90} values in Table 1. Three kinds of glass powders, all having nominally spherical shape were employed. One consisted of solid A-glass particles and the second consisted of hollow borosilicate glass particles having similar sizes. The third was a smaller size silica powder of the kind used in encapsulants for microelectronic devices.

The alumina was dispersed in two epoxy resins differing in rate of cure and, therefore, permitting a greater or lesser extent of particle sedimentation. The slower curing resin consisted of a liquid resin (di-glycidyl ether of bisphenol A kind of epoxy, Shell Epon 828) cured with a mixture of aromatic amines (Curing Agent Z produced by Air Products and Chemicals). The curing kinetics of this epoxy have been characterized [8]. The faster curing resin consisted of a lower molecular weight version of the same resin (Epon 826) cured with a mixture of two amines, a cycloaliphatic type (Ancamine 2049, produced by Air Products and Chemicals) and an aliphatic ether type (Jeffamine D-230, produced by Huntsman Petrochemical).

The glass and silica particles were dispersed in two different epoxy resins. One consisted of the same Epon 828 epoxy cured with diethanolamine, whose curing kinetics are documented [8]. The second epoxy was the same except that it contained 9 wt% of an elastomeric butadiene–acrylonitrile copolymer modifier often added to improve mechanical toughness of epoxies, CTBN 1300X8 [9]. Both these resins contained a very low concentration (<0.01 wt%) of a fluorescent dye, Rhodamine-B. Contrast between fluorescent resin and non-fluorescent particles allowed them to be imaged by laser confocal microscopy, as detailed below.

2.2. Procedures

Specimens for X-ray radiography measurements were 6 mm, parallel-faced slabs of alumina-filled epoxy cut in a vertical orientation from larger castings. For confocal microscopy experiments, small slabs of glass-filled epoxy were mounted and polished using standard metallographic procedures. Unpolished specimens of the hollow-glass-filled epoxy produced poor quality micrographs (even though other polymer composites are said to require no special preparation for confocal microscopy [10]).

X-ray attenuation measurements employed a divergent beam, polychromatic X-ray source. The X-ray tube had a tungsten anode operated at 140 kV with a focal spot size of 0.2×0.2 mm. The beam was filtered by 1 mm beryllium and 16 mm aluminum sheets. Collimators on the X-ray source and detector produced an effective direct-beam-illuminated spot on the specimen having dimension between 0.2 and 0.25 mm, along the direction plotted in the figures to follow. In other words, measurements of X-ray attenuation were obtained with spatial resolution between 0.2 and 0.25 mm.

The laser confocal microscopy was performed using a Bio-Rad MRC-600 laser confocal scanning head mounted on a Nikon Diaphot inverted microscope. The specimen was illuminated with 568 nm light produced by a Krypton–Argon ion laser and a narrow pass filter. This nearly monochromatic excitation light was excluded from the image-forming mechanism by a long-pass 585 nm filter. Only light having wavelength above 585 nm, which arises from fluorescence of the dyed resin, was utilized to produce images. A $40\times$, 1.0 numerical aperture oil-immersion Nikon objective was fitted on the microscope and produced images having lateral dimensions of 420 by 320 μm. A variable aperture on the confocal head was adjusted to produce an optical section thickness of 2 μm [11]. Specimens were translated precisely under the microscope using a micrometer driven, home-made jig. An elaborate discussion on confocal laser scanning microscopy is available in Refs. [12,13].

Scanning electron microscopy backscatter images of the silica-filled epoxy were obtained from a polished surface using a Hitachi S-4500 microscope operating at an accelerating voltage of 15 kV. Prior to microscopy, the surface of each sample had been sputter coated with gold–palladium.

3. Data analysis

Measurements of fractional X-ray transmission through alumina filled epoxy specimens were reduced to filler concentration using calibration specimens having known concentration and the analysis summarized below. The fractional transmission T of the polychromatic radiation passing through a material consisting of two phases A and B (particles and epoxy polymer) is given by

$$\ln(T) = -\bar{\mu}_A t_A - \bar{\mu}_B t_B \tag{2}$$

where $\bar{\mu}$ is the linear attenuation coefficient averaged over the spectrum of the radiation and t is the thickness of a phase. Issues involving averaging over the X-ray spectrum (beam-hardening complications) are accounted for by selecting calibration specimens having nearly the same composition and thickness as the test specimen. If phase B attenuates the radiation much less than A, the last term in Eq. (2) reduces to a constant K_1 having a smaller magnitude than either of the other two terms. That is a reasonable approximation for alumina (A) and epoxy (B) because for 140 keV X-rays, $\bar{\mu}$ for epoxy is 3 times smaller than that for alumina and because the thicknesses of the two phases are similar (as will be seen below). Expressing the thickness of phase A in terms of its volume fraction using a standard stereological relationship [14] and rearranging, permits the last equation to be expressed as

$$\varphi_A = -\bar{\mu}_A^{-1} t^{-1} \ln(T) + t^{-1} K_2 \tag{3}$$

where φ_A is the volume fraction of phase A, t is the specimen thickness and K_2 is a new constant equal to $\bar{\mu}_A^{-1} K_1$.

The two unknowns in Eq. (3), $\bar{\mu}_A^{-1}$ and K_2, were determined from a plot of T measurements on six calibration specimens, each having known thickness t and alumina

volume fraction. The plot followed the expected linear form. Eq. (3) could then be used to determine spatial profiles of alumina volume fraction in a test specimen having known thickness by measuring profiles of the X-ray fractional transmission T.

Regarding determination of the local concentration of particles by microscopy, it is well known that this can be determined from their area fraction on an infinitely thin plane section, as long as the section is representative of the material [14]. If the section thickness is finite, but less than the particle size, the volume fraction φ is related to the area fraction A_A as follows.

$$\varphi = A_A - 1.5\, h/D_{SV} \tag{4}$$

where h is the section thickness and D_{SV} is the surface–volume average diameter of the particles [15], defined as $\sum_i (n_i D_i^3)/(n_i D_i^2)$, where n_i represents number fraction. D_{SV} derived from size distribution measurements on the solid and glass particles is listed in Table 1. Subjectivity involved with determining the area fraction of particles A_A from micrographs was minimized by employing an operator-independent method for segmenting the total area between particles and epoxy. This segmentation utilized an algorithm that performs a statistical t-test on an image brightness histogram. The segmentation algorithm implemented in commercial image analysis software, Image Pro Plus (from Media Cybernetics, LP), was employed in this work.

4. Results

4.1. X-ray attenuation measurements

Fig. 2(a) and (b) show measurements of volume fraction of the alumina particles near the bottom surface of two epoxy specimens. The plots in Fig. 2(a) and (b) show results for the same alumina in a slower and a faster curing epoxy resin, respectively. The transformation from liquid to solid gel occurred after 7.8 h vs. 6.7 h of curing for the slower and faster curing epoxies. This gel transformation arrests sedimentation of alumina particles. In both the plots, increasing abscissa values correspond to increasing distance from the bottom, but the absolute values of abscissa have no significance.

The profile in Fig. 2(a) shows, far from the bottom (at large distance values), a wide region of uniform concentration averaging 0.437 particle volume fraction. This value differs insignificantly (only 1%) from the volume fraction calculated from the weights and densities of the epoxy's constituents, confirming the accuracy of the measurements. The (a) profile also exhibits, close to the bottom, a 0.2 mm layer having higher than average particle concentration. The highest volume fraction measured in that layer is 12% greater than that in the uniform region. The thickness of the sedimented layer is only 0.2% of the total height of the specimen (only a very small part of the total specimen

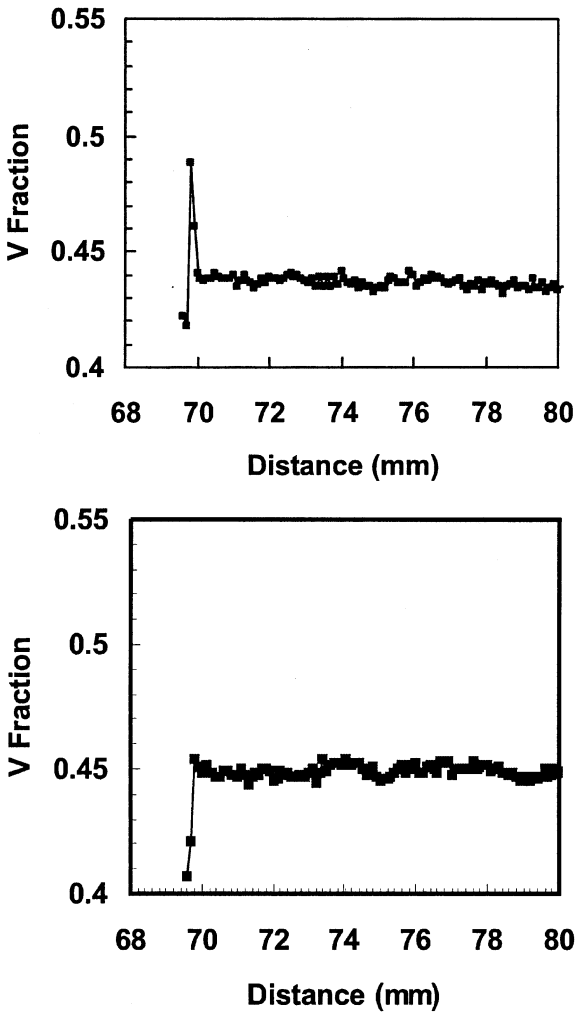

Fig. 2. Concentration profiles measured by radiography near the bottom surface for two epoxy specimens filled with the same alumina particles. Increasing abscissa corresponds to increasing distance from the specimen bottom. The epoxy resin represented in (a) cured more slowly and therefore allowed more time for sedimentation than that represented in (b). The drop in concentration at the extreme left end of both plots is an artifact (see text).

height is shown in Fig. 2). Continuing to still lower abscissa values, the profile exhibits a rapid drop in particle concentration. One likely cause of this experimental artifact is the finite-width X-ray beam straddling the bottom surface of the specimen. Another likely cause is slight misalignment of the beam direction with the specimen edge, which reduces the effective path length causing beam attenuation. In principle, improving the spatial resolution of the particle concentration measurements would improve the accuracy of the concentration profile and probably increase the maximum in measured particle concentration at the specimen bottom. Towards this end, we attempted to measure [16] concentration profiles in alumina filled epoxy materials using a tomographic technique that utilized a synchrotron radiation source (X-ray Tomographic Microscopy [17]). This technique was capable of producing profiles having higher spatial resolution, of the order of 10 μm. These

results will not be presented here because they still contained an edge-related artifact, showing that improved spatial resolution, by itself, does not necessarily solve that problem.

The profile in Fig. 2(b) conforms to the expectation that the same particles should exhibit less particle sedimentation in the faster curing epoxy. The abrupt drop in volume fraction near the bottom surface is again seen, confirming that it is a measurement artifact unrelated to the concentration profile.

4.2. Microscopy images for determining local particle concentration

To determine particle concentration profiles having better spatial resolution and fewer edge-related artifacts than the radiography results, microscopy coupled with image analysis was employed. The main advantage of microscopy over beam attenuation methods is that the particle concentration can be determined close to a specimen edge, as long as that edge and the particle outlines can be unambiguously imaged. A disadvantage of microscopy is that care must be taken to image a statistically representative number of particles at each location within a specimen. The acceptably low experimental scatter in measured particle concentration profiles to be shown below demonstrates that this requirement was satisfied in this work. To simplify the technique development, we initially used optical microscopy. This could resolve neither the smallest particles in the alumina size distribution nor the silica particles used in this work, but it could resolve the solid and hollow glass particles.

Simple, reflected light optical microscopy imaged particle outlines very well for the solid glass particles dispersed in epoxy, but poorly imaged the hollow glass particles. The poor definition of hollow particle outlines in reflection micrographs is shown in Fig. 3(a). However, Fig. 3(b) shows that the fluorescence laser confocal images delineated the hollow particle outlines unambiguously. This excellent contrast between the epoxy and hollow particles in the confocal images is caused by the image being formed exclusively by light from the fluorescing Rhodamine-B dye, present only in the epoxy phase and absent from the glass walls and hollow interiors of the particles. The confocal micrographs imaged the particle outlines for the solid glass particles equally well. Another desirable attribute of confocal microscopy is that the depth of the sampling volume within which particle outlines are imaged (h in Eq. (4)) is small, relative to the particle diameters. For the microscope configuration employed, this depth has been determined previously to be 2 μm [11]. Confocal fluorescence microscopy was therefore employed for measuring concentration profiles for both types of glass particles.

4.3. Concentration profiles from confocal micrographs

Confocal microscopy via its 'optical slicing' feature [12,13] has the capability to characterize material microstructure below the surface of a specimen. Nevertheless, in this work, particle volume fractions were determined from micrographs obtained very close to the specimen surface. The reason is explained using Fig. 4. This shows a plot of volume fractions measured at different depths below the polished specimen surface. The plot for the solid glass particles exhibits ±0.03–0.04 variation in volume fraction with no monotonic trend with increasing depth below the surface. This variation is believed to be caused by experimental scatter in measuring concentration of these particles, because similar scatter is seen in all measurements on this material (see next two figures.) In contrast, the hollow particle results in Fig. 4 show a monotonic increase in concentration at depths greater than 5 microns. This is believed to be caused by an artifact arising from attenuation of fluorescence produced by the dyed epoxy at those depths. Attenuation caused by reflection of light (produced by the dyed epoxy) at the interior walls of the hollow particles is believed to make the dark, non-fluorescing particles appear to be larger in area and therefore have higher concentration. This attenuation is believed to be less severe when the hollow particles are imaged at depths that are a small fraction of their average diameter (40 μm). Fig. 4 suggests that the concentration measurements are

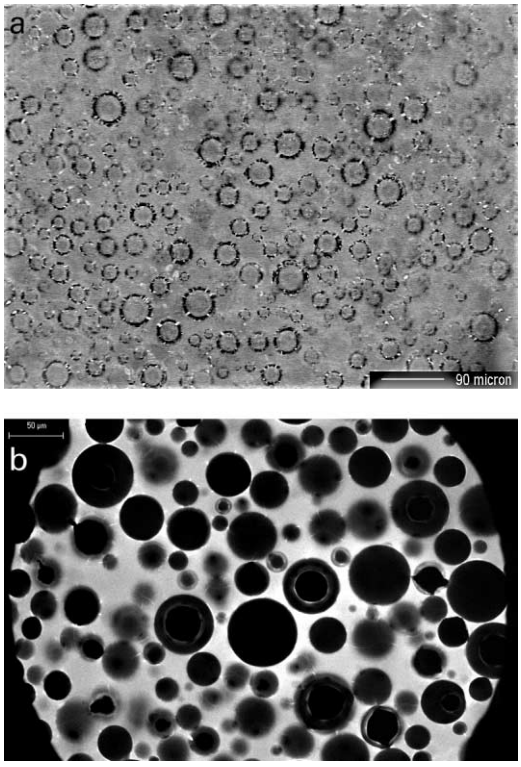

Fig. 3. (a) Reflected light optical micrograph of epoxy filled with the hollow glass particles. This does not clearly delineate the particle outlines. The white bar represents 90 μm. (b) Confocal laser fluorescence micrograph of the same material, showing clearly delineated particle outlines. The white bar represents 50 μm. Using images like that in (b), particle volume fraction was determined within a rectangle 320 μm high in the direction of the gradient and 420 μm wide.

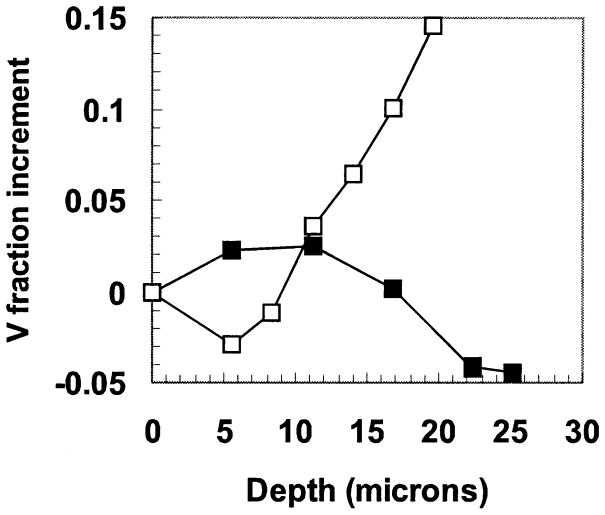

Fig. 4. Dependence of particle volume fraction on depth below the polished surface of a microscopy specimen. The ordinate is the increment in volume fraction from the value at the surface. Closed and open symbols refer to solid and hollow glass particles, respectively.

accurate at depths less than 5 μm for the hollow particles and less than 25 μm for the solid particles. Concentration measurements shown below for both kinds of particles were performed at depths less than 5 μm.

Fig. 5 is a plot of particle concentration vs. height for an epoxy filled with 0.49 volume fraction of solid glass particles (in this and the following figure, the abscissa is height parallel to the gravitational field; the abscissa of Fig. 4 is depth below the surface of a polished specimen, which is perpendicular to gravity). Sedimentation of the particles prior to the epoxy's gel point produced an excess near the bottom surface (at abscissa = 0) and depletion near the top surface, separated by a middle zone of essentially constant concentration. The average concentration of glass particles over the middle zone agrees to within 0.2% with the average volume fraction, computed from the weights and densities of constituents in the filled epoxy (0.49). The apparent asymmetry in the profile, i.e. the more gradual transition from the sedimented zone to the middle zone and the more abrupt transition from the middle zone to the depleted zone, is believed to be a real phenomenon, not a measurement artifact. It can be predicted from a model of particle sedimentation, as explained in Section 5. It should be noted that the results in Fig. 4 were obtained in the middle zone. It should also be noted that the volume fraction results in Fig. 5 do not include the correction suggested by Eq. (4). Including that correction would have decreased the measured particle volume fraction in the middle zone to 0.41, raising the discrepancy with the computed volume fraction to 16%. The applicability of the correction for finite section thickness to these confocal micrographs is discussed below.

Fig. 6 shows profiles for two materials containing different concentrations of the hollow glass particles. Particle flotation produced a depletion zone at abscissa = 0, a middle zone of essentially uniform concentration, and concentrated zone near the top. In the materials having higher and lower initial concentration, the middle zone particle volume fraction agrees with the value computed from weights and densities to within 2 and 3%, respectively. Note that an asymmetry similar to that in Fig. 5 appears to be present in both profiles. That is, both profiles suggest that the transition region between the depleted zone and the middle zone is more abrupt than the transition between the middle zone and the concentrated zone (that asymmetry

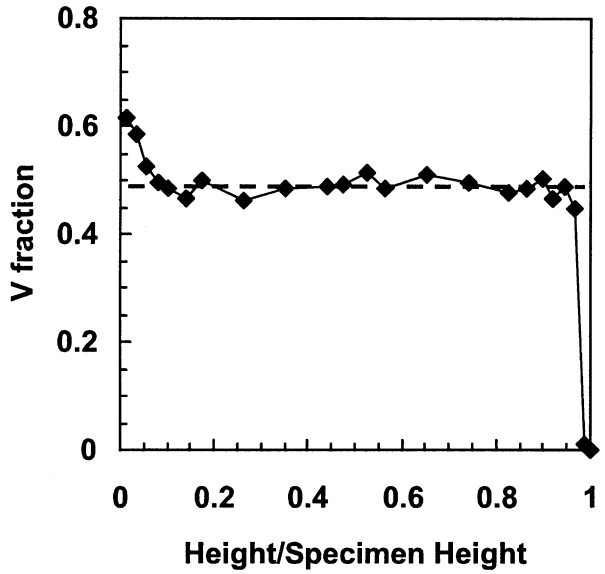

Fig. 5. Concentration profiles for epoxy filled with the solid glass particles. The bottom of the specimen corresponds to 0 on the abscissa and its height was 14 mm. The horizontal line shows the average particle volume fraction of 0.49 computed from weights and densities of constituents.

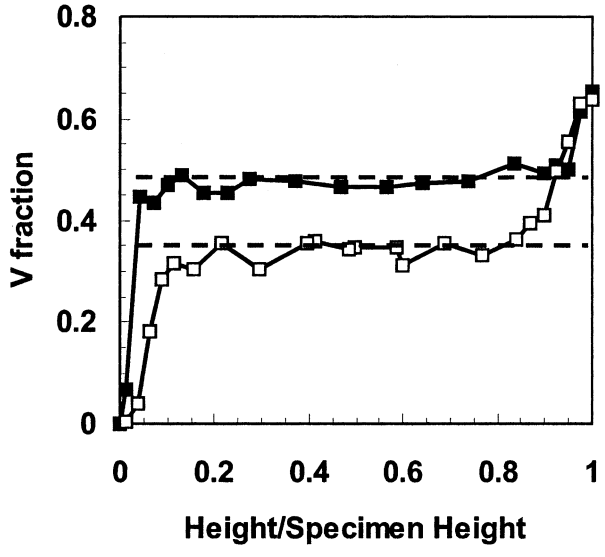

Fig. 6. Concentration profiles for the same epoxy filled with 0.48 and 0.35 volume fraction (filled and open symbols, respectively) of the hollow glass particles. The bottom of each specimen corresponds to 0 on the abscissa and the height of both specimens was 13 mm. The horizontal dashed lines shows the computed average particle volume fractions.

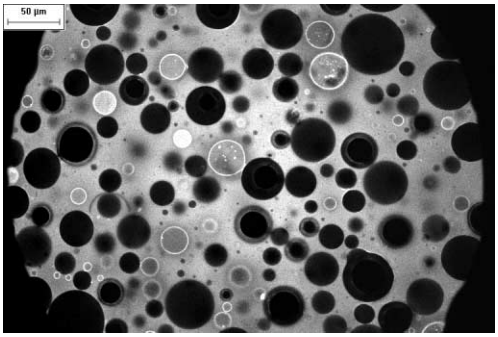

Fig. 7. Confocal laser fluorescence micrograph of an epoxy modified by the CTBN elastomeric particles and filled with 0.48 volume fraction of hollow glass particles. The elastomeric particles are brighter than the glass particles because they have a higher concentration of fluorescent dye. Image analysis produced a concentration of glass particles agreeing with the expected value (see text). The bar represents 50 μm.

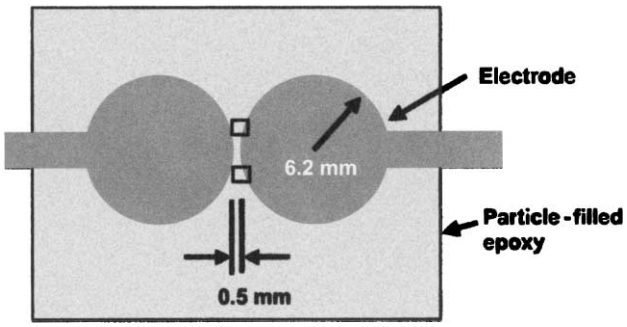

Fig. 8. Schematic representation of two locations in a test specimen at which micrographs in Fig. 9 were obtained. The two spherical electrodes were encapsulated by an epoxy filled with the hollow glass particles. The upper and lower rectangles represent locations near the electrode–epoxy interface that are shown in Fig. 9(a) and (b), respectively. During the encapsulation, the particles floated vertically, opposite to the direction of gravity.

is obscured in the higher concentration epoxy by scatter in measured concentration values near both boundaries). As in Fig. 5, the volume fractions in Fig. 6 do not include the correction for finite section thickness, because that would have worsened the agreement with the known particle concentration in the middle zone.

Many particle reinforced epoxy materials contain elastomeric toughening agents that form a separate population of spherical polymeric particles [18]. The confocal microscopy technique was able to distinguish elastomeric particles in order to determine the concentration of the glass filler particles alone. Fig. 7 shows a confocal micrograph of an epoxy containing the CTBN elastomeric modifier and 0.48 volume fraction of the hollow glass particles. The epoxy materials shown in Figs. 3(b) and 7 are the same except for the CTBN modifier particles. In Fig. 7, the elastomeric particles can be distinguished because they are brighter than the glass particles. The elastomeric particles are brighter because they have a higher concentration of fluorescent dye than the glass particles which contain no dye. Measurements on four images obtained far from specimen boundaries produced an average, glass particle volume fraction (uncorrected by Eq. (4)) of 0.496 ± 0.038, which differs only by 3% from the value computed from the weights and densities of constituents.

We have made use of the confocal microscopy technique for measuring local filler concentration in our laboratory in connection with dielectric breakdown measurements on epoxy materials filled with the hollow glass particles. We needed to determine the particle concentration in a very small volume through which the breakdown propagated, because the breakdown strength of the polymer is reduced considerably by the hollow particles [19]. The dimensions of the material volume are schematically shown in Fig. 8. The breakdown propagated through a 0.5 mm layer of epoxy separating two 12 mm diameter spherical electrodes. We determined a particle volume fraction of 0.445 (with standard deviation of 0.037) in the region close to the center-line axis of symmetry between the electrodes (a region having boundaries 300 μm above and below that axis). The standard deviation was larger than normal because that region, having a minimum width of only about 12 average particle diameters, contained a relatively small number of particles. The concentration within the gap region was not significantly different from the average particle volume fraction of 0.487. However, we did detect non-uniform particle concentration near electrode–epoxy interfaces that had a component of particle flotation velocity oriented along a normal to the interface. Particle depletion near an interface is shown in Fig. 9(a), where the normal component of flotation velocity vector was directed away from the interface. Accumulation of particles is observed in Fig. 9(b), where the normal component of flotation was directed towards the interface, as expected. It was not possible to measure with any accuracy the particle concentration in those two thin layers because they contained a relatively small number of particles. We have used qualitative characterizations of particle concentration profiles like those shown in Fig. 9(a) and (b) and quantitative profiles like those shown in Figs. 5 and 6 to determine the effect of different temperature schedules for curing filled epoxies on particle flotation or sedimentation.

4.4. Local concentration measurements for smaller particles

Filler particles in encapsulants for packaging microelectronics are smaller than the particles used in the preceding experiments. The goal of this portion of the work was to demonstrate feasibility for determining the local concentration of those smaller particles, microscopically. The silica powder listed in Table 1 was selected to represent fillers used in microelectronic encapsulants. Since an appreciable fraction of these particles was smaller than 1 micron, electron microscopy was employed to image them, instead of optical microscopy. Analysis of backscattered scanning electron micrographs (taken far from specimen boundaries)

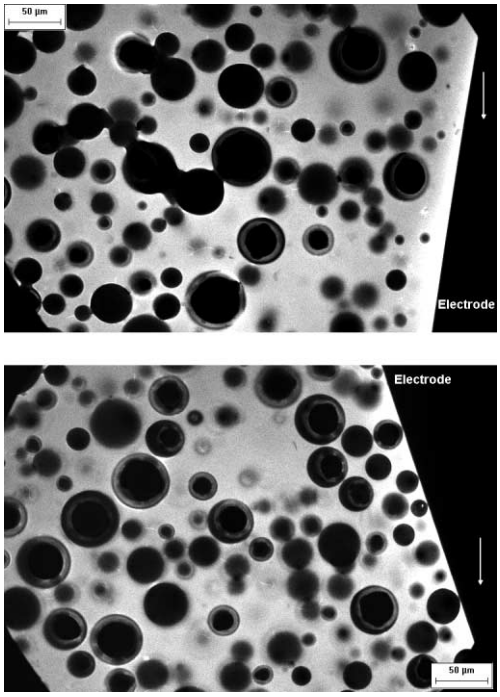

Fig. 9. Confocal micrographs illustrating qualitatively the effect of particle flotation on the concentration profile near the surface of the spherical electrodes shown in Fig. 8. Fig. 9(a) and (b) were obtained near the upper and lower rectangular areas in Fig. 8. The hollow particles floated opposite to the white arrow, which signifies gravity. The upper region, Fig. 9(a), exhibits a layer of depleted particle concentration near the electrode surface, caused by flotation. This depletion zone is absent in the lower region, Fig. 9(b). In both figures, the bar represents 50 μm.

of the silica-filled epoxy produced 0.40 volume fraction of particles. This agreed to within 2% with the volume fraction computed from weights and densities of the constituents. A typical micrograph of this material is shown in Fig. 10.

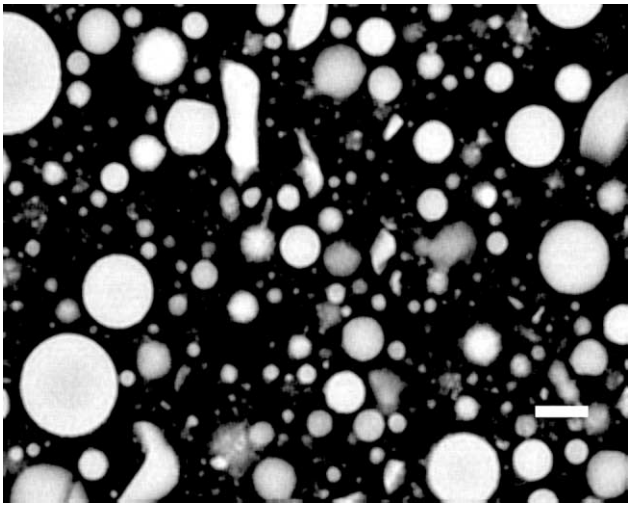

Fig. 10. Scanning electron microscopy backscatter image of the small-size silica particles dispersed in epoxy (without the toughening additive). Analysis of several images produced a particle volume fraction agreeing to within 2% with the known concentration. The white bar represents 2 μm.

Analysis of electron micrographs therefore shows promise for determining profiles of particle concentration in microelectronic encapsulants.

5. Discussions

The X-ray attenuation and microscopy methods are complementary techniques for measuring spatial gradients in particle concentration. Although the attenuation method is prone to an artifact very close to a material boundary, it has several advantages: the particle outlines need not be resolved microscopically, the method is more amenable to automation, and it is less affected by statistical counting errors at low particle concentrations. The main advantage of the microscopy method is that it is less likely to produce systematic errors in particle concentration close to material boundaries, where concentration gradients are usually most severe. The fundamental origins of this advantage are that microscopy can identify a specimen boundary more reliably, because with microscopy, the sampling volume has much smaller thickness. In contrast, the necessarily larger thickness of specimens for the attenuation method make it prone to errors caused by imperfect alignment of the beam along the specimen edge.

The precision, or experimental uncertainty, in the particle volume fraction measurements can be estimated from the standard deviation of the individual measurements in the middle zone, where the volume fraction is constant. These standard deviations of volume fraction are 0.002 for the attenuation-derived measurements in Fig. 2, 0.015–0.02 for the optical microscopy measurements in Figs. 5 and 6 and 0.028 for the electron microscopy measurements on the small silica particles. The corresponding uncertainties on the mean of 10 volume fraction measurements in the middle zone can be computed from those standard deviations to be ± 0.0015, ± 0.01–0.015 and ± 0.02, respectively. Considering these uncertainties, the mean particle volume fractions measured in the middle zones of each material (values listed in Section 4) agree with values computed from weights and densities of the particle and epoxy phases. The scatter in the measured concentration of the hollow particles in Fig. 6 appears to be larger than that for the solid particles in Fig. 5, probably because the former is worsened by inaccuracies caused by reflections of the fluorescing light from internal surfaces in the hollow particles, discussed above.

It should be noted that the accuracy of the volume fractions from microscopy refers to results uncorrected by the finite-slice-thickness term in Eq. (4). Inclusion of this term would have reduced the average volume fraction in the middle zone of Figs. 5 and 6 by 0.08 volume fraction, causing a statistically significant disagreement with the computed volume fractions. It is therefore concluded that the finite thickness correction is not appropriate for volume fraction measurements of the solid and hollow glass particles by the confocal fluorescence microscopy

technique. This observation cannot be explained. In contrast, the particle concentration results derived from scanning electron micrographs require no finite-thickness correction since they image the flat, polished surface of a specimen, instead of a section having finite thickness.

The asymmetry in the particle concentration profiles shown in Figs. 5 and 6 is consistent, at least qualitatively, with theory for sedimentation (or flotation) of particles. The experimentally observed asymmetry is discerned by a gradient in concentration that is larger in absolute value (steeper slope) at the transition between the clear zone and the middle zone than at the transition between the middle zone and the maximum packed zone. In other words, the rise in concentration between the clear zone and the middle zone appears to be more abrupt than the rise in concentration between the middle zone and the maximum packed zone. This asymmetry was observed for the case of sedimenting particles in Fig. 5, as well as for floating particles in Fig. 6, although the larger scatter in the hollow particle concentration profiles in Fig. 6 somewhat obscures the asymmetry. This asymmetry is consistent with the theory of gravitationally driven particle sedimentation, derived for particles large enough that hydrodynamic and gravitational forces dominate over interparticle and Brownian forces [3,4,20]. For the case of a fluid having an initially uniform concentration of *single-size, monodisperse particles*, theory shows that the rise in concentration from the middle zone having the initial concentration to the maximum packed zone can never be abrupt, unless the initial concentration prior to sedimentation is either very close to the concentration in the clear zone, 0, or very close to the concentration in the maximum packed zone. This restriction, explained in the next paragraph, is a consequence of a mass balance of particles at the interface between the middle and packed zones. In contrast, theory shows that the rise in concentration from the clear zone to the middle zone can always be abrupt (a discontinuous step), regardless of the initial concentration. Therefore, sedimentation theory for monodisperse particles predicts that the rise in concentration from the clear to the middle zone can be more abrupt than the rise from the middle to the maximum packed zone, qualitatively consistent with the results in Figs. 5 and 6. We believe that this sedimentation behavior of monodisperse suspensions is the underlying cause for the experimentally observed asymmetry in concentration profiles for the polydisperse particles we analyzed.

The theory-based restriction on the shape of the concentration profile in the region between the middle and maximum packed zones will now be described more quantitatively. It has been shown [3,4,20] that a discontinuous jump in concentration between these two zones will satisfy particle mass continuity only if the particle flux and the concentration in the middle zone satisfies a requirement shown in Fig. 11. This shows a plot of the dimensionless particle flux $\varphi U(\varphi)/U_s$, which is the volume fraction φ times the particle sedimentation velocity U normalized by

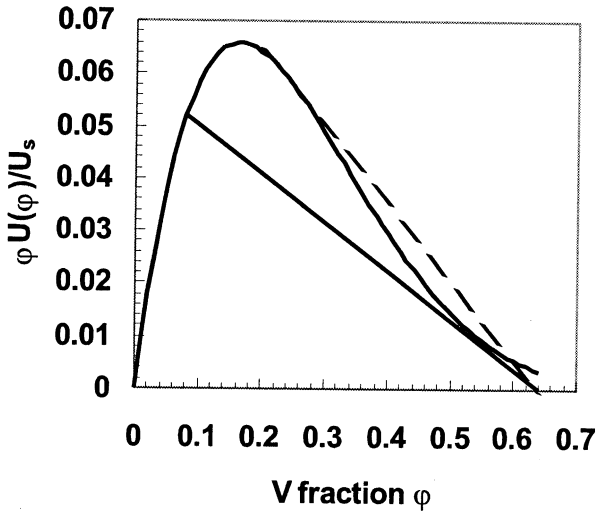

Fig. 11. A plot of the dimensionless sedimentation flux $\varphi U(\varphi)/U_s$ prepared using Eq. (5) with $n = 5.1$ for the hindered settling function $U(\varphi)/U_s$. The lines connect the point corresponding to the maximum packed zone at volume fraction $\varphi_m = 0.64$ with two points on the flux curve corresponding to different initial particle concentrations, $\varphi_0 = 0.08$ (solid) and 0.2 (dashed.) The case of 0.08 initial concentration allows a discontinuous jump in particle concentration from the middle zone to the maximum packed zone, but the 0.2 initial concentration does not, for reasons explained in the text.

the Stokes velocity (the limiting sedimentation velocity for infinitely dilute particles) U_s. The so-called hindered settling function $U(\varphi)/U_s$ employed to make the plot in Fig. 11 follows a form applicable to non-colloidal particles having size comparable to the solid and hollow glass spheres employed in this work

$$U(\varphi)/U_s = (1 - \varphi)^n \tag{5}$$

where typical values of n are 4.6 and 5.1 [3,20–22]. The latter value was used to prepare Fig. 11, and the former value would give a curve having a similar shape. The requirement of particle flux continuity at the interface between middle and packed zones exhibiting a discontinuity in particle concentration, is as follows. It is required that in Fig. 11 the straight line connecting the point representing the middle zone (having abscissa φ_0 and ordinate $\varphi_0 U(\varphi_0)/U_s$) and the point representing the packed zone (having abscissa and ordinate φ_m and 0) must have an ordinate value that is never higher than the ordinate value of the flux curve $\varphi U(\varphi)/U_s$ (the slope of that straight line is the velocity by which the discontinuity propagates through the sedimenting fluid). The solid line in Fig. 11 illustrates a middle zone (initial) volume fraction of 0.08 that is consistent with a discontinuous jump to the packed zone concentration of 0.64, and the dotted line illustrates a middle zone concentration of 0.2 that could not satisfy particle continuity if the concentration profile had a discontinuous jump. The values of initial (middle zone) concentration that would allow a discontinuous jump in concentration between the middle and packed zones has been determined numerically

for the hindered settling function in Eq. (5). For an n value of 4.6 or 5.1, a discontinuous jump is not allowed if the initial particle volume fraction in the middle zone is in the range 0.15–0.50 or 0.09–0.53, respectively (an alternative form of the hindered settling function, Eq. (2.1) in a review by Davis and Acrivos [21], gave a similar result for the excluded range, 0.11–0.55). The initial volume fractions for the experimental cases shown in Fig. 5, 0.49, and Fig. 6, 0.48 and 0.35, are in the disallowed range for all three hindered settling functions; therefore, a discontinuous jump from the middle zone to the packed zone would not be allowed for the case of monodisperse particles. It should be recalled that the same theory allows a discontinous jump from the clear zone to the middle zone for all values of initial concentration (that is intuitively reasonable, since monodisperse, sedimenting particles initially at the top of the middle zone, all moving at the same velocity should produce a sharp boundary between clear and middle zones [20]). It is believed that the physics captured in this theory for monodisperse particles is the cause of the experimental observation that the concentration profile varies less abruptly between the middle and packed zones than between the clear and middle zones. Fluid-mechanics based simulations of particle sedimentation/flotation in curing polymers, recently performed by collaborators in our laboratory, also exhibit the aforementioned asymmetry [23].

6. Conclusions

Particle concentration profiles in polymers have been measured by X-ray beam attenuation and microscopy techniques. Confocal scanning optical microscopy was employed for particles larger than 10 μm, and beam attenuation was employed for smaller particles. The spatial resolution of the attenuation-derived concentration measurements is controlled mainly by the effective diameter of the beam. That is influenced by several characteristics of the apparatus, such as the sizes of collimators on the incident beam and on the detector, which makes the resolution somewhat uncertain. The spatial resolution of the microscopically derived concentration measurements is easier to define, since it depends only on the dimensions of a counting area. In our experiments on 40 μm particles, measurements from images 320 μm long (in the gradient direction) produced concentration profiles, which agreed with expectations. For example, an asymmetry expected in profiles produced by sedimentation was observed by the microscopic technique. Near a specimen boundary, local concentration determined by the beam-attenuation method is prone to an artifact caused by geometric and alignment issues, but this artifact is absent from the microscopic method. This is an important distinction for determining particle concentration gradients, because the gradients are usually most severe near boundaries. Although most of the microscopic results were obtained on particles having sizes of tens of microns, local concentration of the smaller particles used in microelectronic encapsulants appeared to be measurable by imaging the particles via electron microscopy instead of optical microscopy.

Acknowledgements

S. Stricker and M. Folsom of the University of New Mexico made available a laser confocal microscope and provided valuable guidance. J. Schroeder, B. McKenzie and A. Antolak of Sandia National Laboratories performed the particle size measurements, scanning electron microscopy and X-ray Tomographic Microscopy. C. Romero, L. Mondy, R. Rao and A. Sun of Sandia advised the authors on hindered settling functions.

Sandia is a multiprogram laboratory operated by Sandia Corporation, a Lockheed Martin Company, for the United States Department of Energy under Contract DE-AC04-94AL85000.

References

[1] Pecht MG, Nguyen LT, Hakim EB. Plastic encapsulated microelectronics. New York: Wiley-Interscience, 1995.
[2] Driscoll T, Li P, Lehmann G, Cotts E. In: Groothuis S, Ho P, Ishida K, Wu T, editors. Electronic packaging materials science IX, Materials Research Society Symposium Proceedings, vol. 445. Materials Research Society, 1997. p. 69–74.
[3] Russel WB, Saville DA, Schowalter WR. Colloidal dispersions. Cambridge: Cambridge University Press, 1989.
[4] Auzerais FM, Jackson R, Russel WB. J Fluid Mech 1988;195:437–62.
[5] Shapiro AP, Probstein RF. Phys Rev Lett 1992;68:1422–5.
[6] Leighton D, Acrivos A. J Fluid Mech 1987;181:415–39.
[7] Papathanasiou TD. Int Polym Process 1996;11:275–83.
[8] Adolf D, Chambers R. Polymer 1997;38:5481–90.
[9] Sayre JA, Assink RA, Lagasse RR. Polymer 1981;22:87–94.
[10] Thomason JL, Knoester A. J Mater Sci Lett 1990;9:258–62.
[11] Gard DL. In: Matsumoto B, editor. Methods in cell biology, vol. 38. New York: Academic Press, 1993. p. 241–64.
[12] Ribbe AE. Trends Polym Sci 1997;5:333–7.
[13] Sheppard CJR, Shotton DM. Confocal laser scanning microscopy. Oxford: Bios Scientific Publishers, 1997.
[14] Russ JC. Practical stereology. New York: Plenum Press, 1986.
[15] Allen T. Particle size measurement. London: Chapman & Hall, 1990.
[16] Antolak AJ, Lagasse RR. Unpublished results, Sandia National Laboratories, 1997.
[17] Kinney JH, Nichols MC. Annu Rev Mater Sci 1992;22:121–52.
[18] Nakamura Y, Uenishi S, Kunishi T, Miki K, Tabata H, Kuwada K, Suzuki H, Matsumoto T. IEEE Trans Component Hybrids Manufactur Technol 1987;CHMT-12:502–6.
[19] Anderson RA, Lagasse RR, Schroeder JL. Effects of void size and gas content on electrical breakdown in lightweight, mechanically compliant, void-filled dielectrics. J Appl Phys, submitted for publication.
[20] Wallis GB. One-dimensional two-phase flow. New York: McGraw-Hill, 1969. Chapter 8.
[21] Davis RH, Acrivos A. Annu Rev Fluid Mech 1985;17:91–118.
[22] Garside J, Al-Dibouni M. Ind Engng Chem Process Des Dev 1977;16:206–14.
[23] Sun A, Rao R, Mondy L. Private communication, Sandia National Laboratories, 1999.